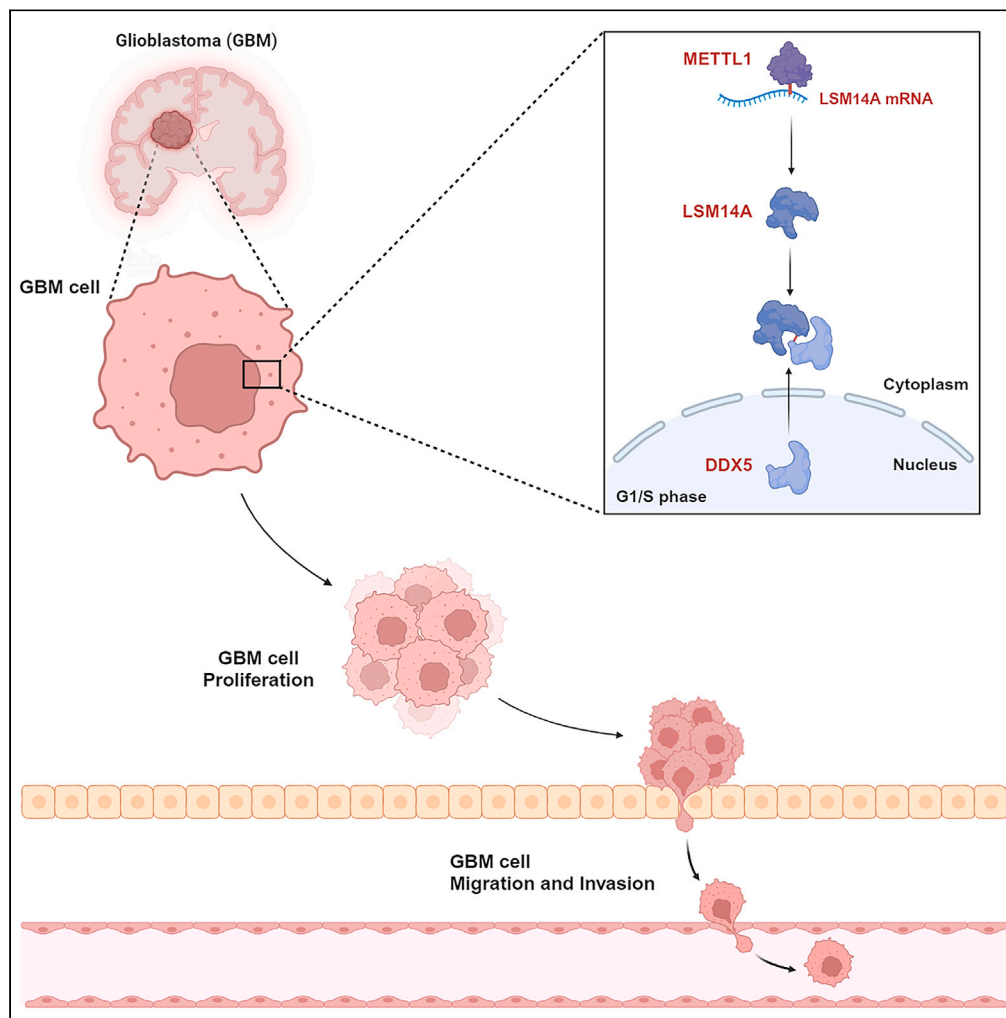


Article

METTL1-modulated LSM14A facilitates proliferation and migration in glioblastoma via the stabilization of DDX5



Changyu Wang,
Yan He, Xiang
Fang, ..., Shuxin
Zhao, Lun Li,
Guangyu Li

liguangyu1972@sina.com

Highlights

LSM14A overexpression in GBM promotes tumor growth, in turn affecting GBM prognosis

LSM14A is modulated by METTL1 via m⁷G methylation in GBM

LSM14A stabilizes cytoplasmic DDX5 in G1/S phase to regulate GBM cell cycle progression

Wang et al., iScience 27,
110225
July 19, 2024 © 2024 The
Authors. Published by Elsevier
Inc.
[https://doi.org/10.1016/
j.isci.2024.110225](https://doi.org/10.1016/j.isci.2024.110225)



Article

METTL1-modulated LSM14A facilitates proliferation and migration in glioblastoma via the stabilization of DDX5

Changyu Wang,^{1,7} Yan He,^{2,7} Xiang Fang,³ Danyang Zhang,⁴ Jinhai Huang,¹ Shuxin Zhao,⁵ Lun Li,⁶ and Guangyu Li^{1,8,*}

SUMMARY

Glioblastoma (GBM) is characterized by aggressive growth, invasiveness, and poor prognosis. Elucidating the molecular mechanisms underlying GBM is crucial. This study explores the role of Sm-like protein 14 homolog A (LSM14A) in GBM. Bioinformatics and clinical tissue samples analysis demonstrated that overexpression of LSM14A in GBM correlates with poorer prognosis. CCK8, EdU, colony formation, and transwell assays revealed that LSM14A promotes proliferation, migration, and invasion in GBM *in vitro*. *In vivo* mouse xenograft models confirmed the results of the *in vitro* experiments. The mechanism of LSM14A modulating GBM cell proliferation was investigated using mass spectrometry, co-immunoprecipitation (coIP), protein half-life, and methylated RNA immunoprecipitation (MeRIP) analyses. The findings indicate that during the G1/S phase, LSM14A stabilizes DDX5 in the cytoplasm, regulating CDK4 and P21 levels. Furthermore, METTL1 modulates LSM14A expression via mRNA m⁷G methylation. Altogether, our work highlights the METTL1-LSM14A-DDX5 pathway as a potential therapeutic target in GBM.

INTRODUCTION

Glioblastoma (GBM) is the most prevalent and aggressive central nervous system primary brain tumor.¹ Known for its swift growth and potent infiltration, GBM presents significant clinical challenges.² Despite recent advances in the pathology, biology, and genetics of GBM, the five-year survival rate persists at a mere 5%.³ The low survival rate of GBM arises from its heterogeneity, complex microenvironment, and inherent resistance to conventional treatments.⁴ While emerging therapies, such as molecular targeting, show potential in some tumors, their effectiveness against GBM is still limited.⁵ It is critical to understand the molecular mechanisms of GBM to pave the way for innovative therapeutic targets and strategies.

LSM14A is a crucial component of the mRNA processing body (P-body) and stress granule (SG).⁶ The P-body and SG represent conserved messenger ribonucleoprotein (mRNP) complexes, where the P-body is considered the cytoplasmic focal point for mRNA translational repression and degradation. SG particles safeguard mRNA from damage and prevent the buildup of defective proteins under stress.⁷ Early studies identified LSM14A as an RNA-binding protein that assists in the assembly of the P-body and SG through protein-protein interactions,^{8,9} thereby playing a role in mRNA biogenesis.¹⁰ Furthermore, LSM14A plays a vital role in recognizing viral genetic material and facilitating the innate immune response.¹¹ Crucially, LSM14A is implicated in tumor development. In HeLa cells, LSM14A facilitates mitotic progression.¹² Recent research has demonstrated that LSM14A is highly expressed in hepatocellular carcinoma and is correlated with poor patient prognosis. Moreover, the knockdown of LSM14A inhibits the proliferation of hepatocellular carcinoma cells.¹³ However, the specific mechanism through which LSM14A promotes tumor cell proliferation remains unclear.

The DEAD-box protein family member DDX5, also known as p68, is a central component in RNA metabolism, playing a crucial role in various cellular processes, such as transcription, pre-mRNA and rRNA processing, and miRNA processing.¹⁴ DDX5 has been identified as an oncogene, with notable overexpression in 92.8% of human cancers,¹⁵ including non-small cell lung cancer,¹⁶ breast cancer,¹⁷ gastric cancer,¹⁸ and glioma.¹⁹ The stability of DDX5 is crucial for maintaining the oncogenic characteristics of cancer cells.^{20,21} Additionally, DDX5 plays a significant role in mechanisms such as cell-cycle arrest, DNA repair, and fostering innate immunity against viral infections in cancer

¹Department of Neurosurgery, The First Hospital of China Medical University, NO. 155 Nanjing North Street, Heping District, Shenyang 110002, China

²Department of Laboratory Animal Science, China Medical University, 110122, No. 77 Puhe Road, Shenyang North New Area, Shenyang, Liaoning Province, P.R. China

³Department of Neurosurgery, Central Hospital Affiliated to Shandong First Medical University, No. 105, Jiefang Road, Jinan, Shandong, People's Republic of China

⁴Department of Immunology, College of Basic Medical Sciences of China Medical University, 110122, No. 77 Puhe Road, Shenyang North New Area, Shenyang, Liaoning Province, P.R. China

⁵The Fourth Affiliated Hospital of China Medical University, Shenyang 110032, China

⁶Department of Neurosurgery, Anshan Hospital of the First Hospital of China Medical University, Anshan, China

⁷These authors contributed equally

⁸Lead contact

*Correspondence: liguangyu1972@sina.com

<https://doi.org/10.1016/j.isci.2024.110225>



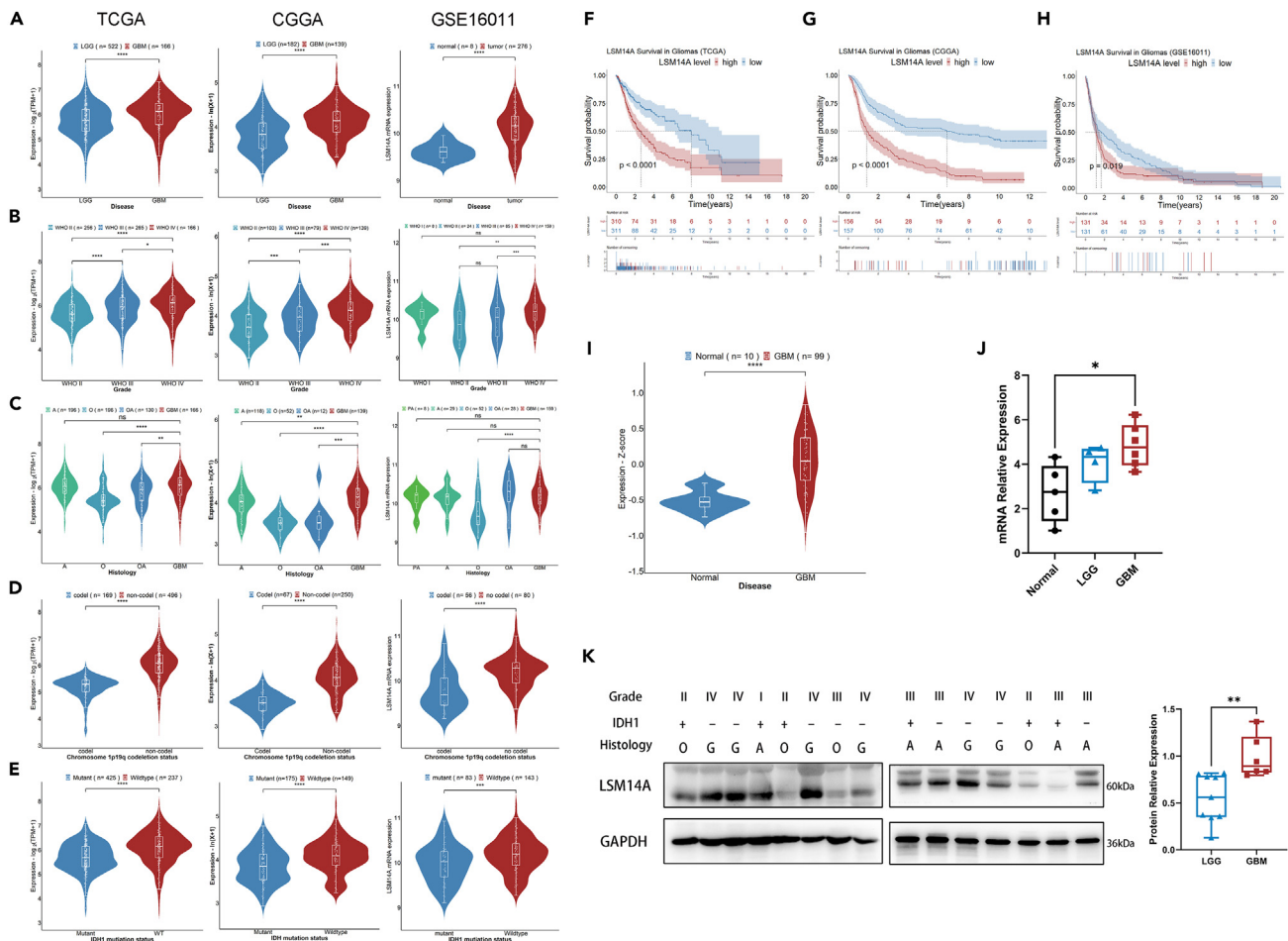


Figure 1. LSM14A expression in gliomas

(A–E) mRNA levels of LSM14A from TCGA, CGGA, and GSE16011 datasets categorized by disease, WHO classification, tissue type, IDH mutation, and 1p/19q codletion.

(F–H) Kaplan-Meier survival curves for glioma patients from the TCGA, CGGA, and GSE16011 datasets stratified by LSM14A expression levels.

(I) LSM14A protein levels variation between the normal and GBM groups in the PDC000204 dataset.

(J) LSM14A mRNA levels in glioma tissues, analyzed via RT-qPCR.

(K) Protein levels of LSM14A in glioma samples, ascertained via immunoblotting (“A”: astrocytoma, “O”: oligodendrogloma, “OA”: oligoastrocytoma). The data are represented as the mean ± S.D. of three independent experiments. ns = not significant, **p* < 0.05, ***p* < 0.01, ****p* < 0.001, *****p* < 0.0001.

contexts.²² For example, DDX5 promotes G1/S phase transition and proliferation in breast cancer cells.²³ In gliomas, DDX5 has been pinpointed as a facilitator of tumorigenesis, encouraging both proliferation and invasion.^{24–26} These studies propose that targeting DDX5 could restrain the malignant progression of gliomas, positioning DDX5 as a promising target for therapeutic interventions.

In this study, we observed high expression of LSM14A in GBM, which positively correlates with adverse patient outcomes, significantly contributing to the proliferation and migration of GBM cells *in vitro*. We demonstrated that within the cytoplasm of cells during the G1/S phase, LSM14A accelerates cell cycle progression by binding to and bolstering the stability of the DDX5 protein. Methyltransferase-like 1 (METTL1), a facilitator of m⁷G methylation in RNA,^{27,28} is significantly overexpressed in GBM²⁹ and is associated with mRNA translocation, stability, and translation in SG.³⁰ Our previous research identified METTL1 as an oncogenic factor in gliomas that influences proliferation in GBM cell *in vitro*.³¹ We found that LSM14A expression is regulated by METTL1. Our results suggest that the METTL1-LSM14A-DDX5 axis plays a critical role in GBM cell proliferation and migration, presenting a potential prognostic and therapeutic target for GBM.

RESULTS

Elevated LSM14A expression in gliomas correlates with poor patient prognosis

To explore the expression and prognostic significance of LSM14A in glioma, we analyzed mRNA data from TCGA, CGGA, and GSE16011. Elevated LSM14A expression was evident in advanced WHO-classified gliomas (Figure 1A–C), non-1p/19q codeletions (Figure 1D), and

isocitrate dehydrogenase (IDH) wild-type gliomas (Figure 1E). High LSM14A expression negatively impacted patient survival rates (Figure 1F–H). The PDC000204 dataset showed elevated levels of LSM14A protein expression in GBM versus normal tissues (Figure 1I). RT-qPCR revealed increased LSM14A mRNA in grade IV gliomas compared with normal tissues (Figure 1J). Western blotting confirmed enhanced LSM14A protein in grade IV gliomas (GBM) compared to low-grade counterparts (Figure 1K). Additionally, LSM14A exhibited high expression in IDH wild-type samples (Figure S1A). Collectively, these data suggest the oncogenic role of LSM14A in glioma.

Impact of LSM14A modulation on GBM cell proliferation and migration

To explore the function of LSM14A in GBM, we assessed its expression in GBM cell lines (U87, U251, LN229, and U118) through immunoblotting. We found LSM14A significantly increased in U87 and U251 compared to LN229 and U118, with all GBM cell lines showing higher levels than normal human microglia cells, HEB (Figure S1B). In response, we modulated LSM14A levels by employing knockdown or knockout strategies in U87 and U251 cells and upregulating it in LN229 and U118. Immunoblotting indicated a marked LSM14A reduction in U87 and U251 cells with LSM14A-KD1 and LSM14A-KD2 (Figure 2A). LSM14A protein was successfully knocked out in U87 and U251 cells, resulting in LSM14A-KO cells (Figures S1C and S1D). Assays including CCK-8, EdU, and colony formation indicated a significant reduction in cell proliferation in U87 and U251 after LSM14A knockdown (Figures 2B–2D). Gene set enrichment analysis (GSEA) analysis, based on TCGA LSM14A expression data, associated the reduced proliferation with the cell cycle pathway (Figure S1E). Flow cytometric analysis showed that LSM14A downregulation blocked the G1/S phase transition in U87 cells (Figure 2E). Additionally, transwell (Figure 2F) and wound healing (Figure S1F) assays demonstrated a reduction in migration of GBM cells subsequent to LSM14A downregulation, and the invasive capacity was notably decreased (Figure S1G). Similarly, in LSM14A-KO cells, assays including CCK-8 (Figure 2G), EdU (Figure 2H), and transwell (Figure 2I) highlighted a more pronounced decline in proliferation and migration in GBM. For LN229 and U118 cells, LSM14A overexpression was successfully established (Figure 3A), leading to a significant increase in cell proliferation, as indicated by CCK-8, EdU, and colony formation assays (Figures 3B–3D). Additionally, there was an increase in migration, as demonstrated by transwell (Figure 3E) and wound healing assays (Figure S1F), along with a rise in invasive capacity (Figure S1G). *In vivo* studies with LSM14A-KD1 and LSM14A-OE in subcutaneous GBM xenograft models revealed a marked reduction in tumor volume in U87 cells with LSM14A downregulation, while LSM14A overexpression led to increased tumor volume in LN229 cells (Figure 3F). Overall, our data highlight the critical role of LSM14A in regulating GBM cell proliferation and migration, associating its function with the cell cycle pathway, and demonstrating that LSM14A downregulation significantly impacts the G1/S phase transition in GBM cells.

DDX5 as a potential interactor of LSM14A

To identify LSM14A-binding proteins, we applied mass spectrometry. Using a control IgG group, 77 proteins with LSM14A affinity were found (Table S3). From PDC000180 and PDC000204 datasets, 616 and 622 proteins correlated highly with LSM14A. The intersection of these data revealed HNRNPDL, DDX5, NCL, and GTF2I as potential LSM14A-interacting proteins (Figure 4A). Their significance in GBM was highlighted by differential expression evaluations across the TCGA, CGGA, GSE16011, and PDC000204 datasets. Specifically, in PDC000204, all four proteins were upregulated in GBM (Figure S2A). In TCGA and GSE16011, all except HNRNPDL exhibited increased expression (Figures S2B and S2C), while only DDX5 and NCL were accentuated in CGGA (Figure S2D). Based on these findings, our analysis particularly emphasized DDX5 and NCL due to their consistently high expression across the four datasets. Our findings demonstrate a significant association between LSM14A and the cell cycle pathway, with its knockdown resulting in G1/S phase arrest in GBM cells. Concurrently, other studies have emphasized the role of DDX5 in facilitating the G1/S phase transition and in promoting tumor cell proliferation. Therefore, DDX5 was identified as a possible LSM14A-interacting protein. We confirmed LSM14A and DDX5 correlation in PDC000180 and PDC000204. A strong LSM14A and DDX5 correlation emerged (Figures 4B and 4C). However, RT-qPCR analysis showed that LSM14A knockdown in U87 cells did not affect DDX5 mRNA levels (Figure 4D). Immunoblotting showed decreased DDX5 after LSM14A knockdown in U87 or U251 and increased DDX5 with LSM14A overexpression in LN229 (Figure 4E). Studies have shown that DDX5 regulates the expression of the important cell cycle regulators CDK4 and P21.^{32–34} Therefore, we investigated whether LSM14A also affects the expression of CDK4 and P21. Immunoblotting showed LSM14A knockdown or knockout decreased CDK4 and increased P21 protein levels. Overexpressing LSM14A in LN229 cells showed opposite effects (Figure 4F). This evidence suggests that LSM14A interacts with DDX5 and regulates the protein levels of DDX5, CDK4, and P21.

LSM14A interacts with nuclear-exiting DDX5 and regulates DDX5 protein stability

We then investigated how LSM14A interacts with DDX5 and regulates its protein levels. We conducted immunofluorescence (IF) experiments on U87 and U251 cells to examine the cellular localization of LSM14A and DDX5. The data indicated that in serum-starved (G0 phase) GBM cells, DDX5 was primarily nuclear, and LSM14A was chiefly cytoplasmic, with no evident colocalization detected between them. In normally cultured GBM cells, DDX5 was found in the cytoplasm, and LSM14A exhibited significant colocalization with DDX5, more so than in serum-starved GBM cells (Figure 4G). To further validate these findings, LSM14A was either knocked down in U87 cells or overexpressed in LN229 cells, and subsequent IF assays were performed to verify the intracellular localization of LSM14A and DDX5 (Figure S2E). Subcellular fractionation experiments in U87 cells confirmed DDX5's localization across various cell cycles (Figure S2F). Additionally, we confirmed their potential protein-protein interactions during specific cell cycles using coIP experiments. The results revealed limited interaction between LSM14A and DDX5 in serum-starved U87 cells (Figure S2G–S2H). In contrast, their interaction intensified in normally cultured GBM cells (Figure 4H). Our experiments show that the influence of LSM14A is limited to the protein level of DDX5, suggesting that the regulatory effect of LSM14A

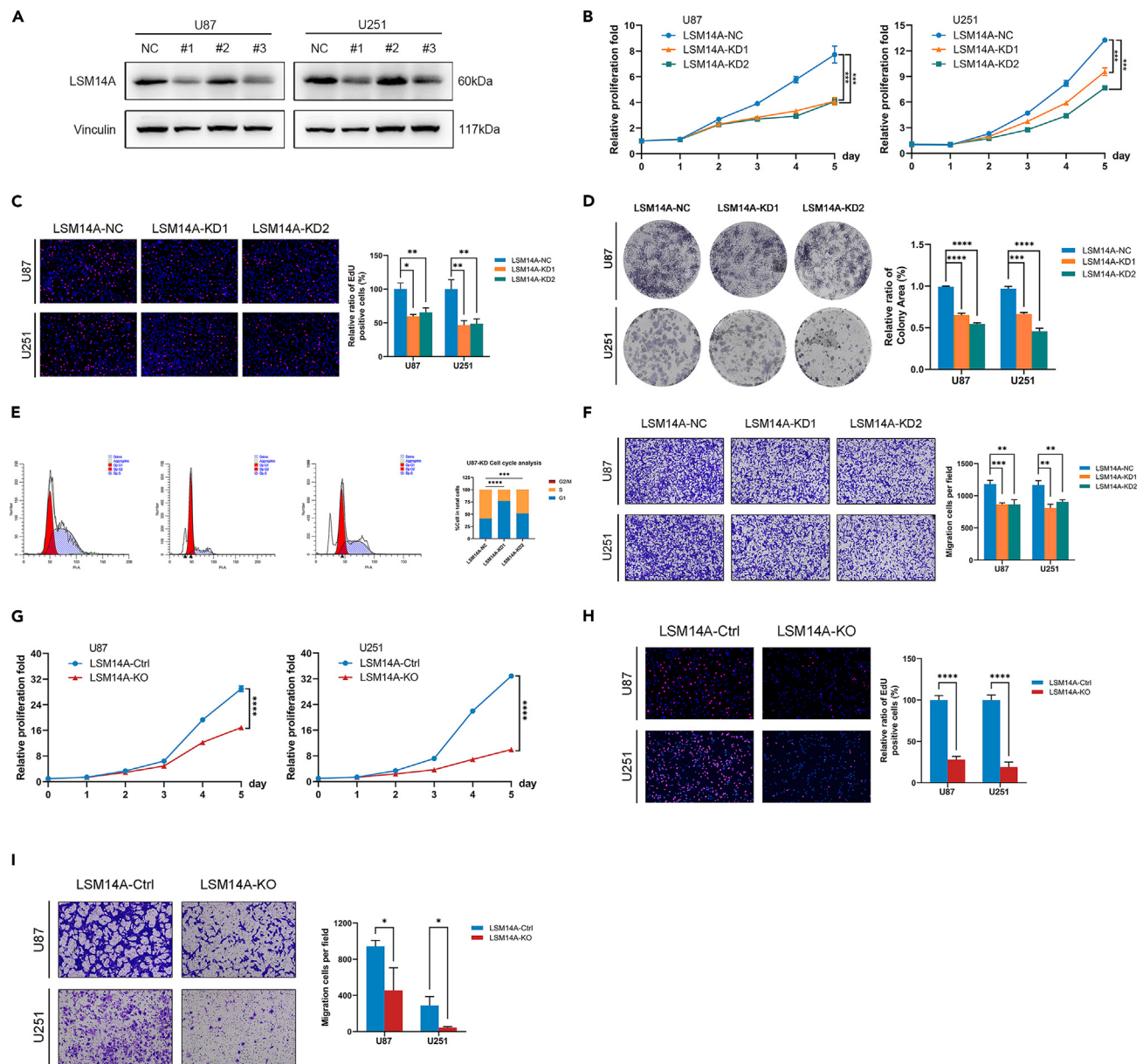


Figure 2. Inhibition of GBM cell proliferation and migration by LSM14A reduction

(A) Efficiency of LSM14A silencing at the protein level in U87 and U251 cells, utilize shLSM14A #1 and shLSM14A #3 to construct LSM14A-KD1 and LSM14A-KD2, respectively.

(B–D) Proliferation in LSM14A-knockdown U87 and U251 cells, as evaluated by CCK-8 (B), EdU (C), and colony formation assays (D).

(E) Flow cytometric analysis of cell cycle distribution in LSM14A-knockdown U87 cells.

(F) Transwell migration assay for LSM14A-NC, LSM14A-KD1, and LSM14A-KD2 groups in U87 and U251 cells.

(G and H) Proliferation assays (CCK-8 [G] and EdU [H]) for LSM14A-KO U87 and U251 cells.

(I) Transwell assay evaluating migration in LSM14A-KO U87 and U251 cells. The data are represented as the mean \pm S.D. of three independent experiments.

* $p < 0.05$, ** $p < 0.01$, *** $p < 0.001$, **** $p < 0.0001$.

on DDX5 occurs post-transcriptionally. Previous studies have shown that LSM14A can bind to various proteins, stabilizing their localization in the cytoplasm.^{35–37} To ascertain whether LSM14A enhances the protein stability of DDX5, we assessed DDX5 abundance in LSM14A-deficient GBM cells and controls, both treated with cycloheximide (CHX). The CHX chase assay is widely used to determine the half-life of proteins in eukaryotes. Immunoblotting indicated that the protein half-life of DDX5 was notably reduced in LSM14A-deficient U87 and U251 cells. Conversely, the DDX5 protein was considerably stabilized in LSM14A-rich LN229 cells (Figure 4I and Figure S2I). Our findings suggest a cytoplasmic interaction between LSM14A and DDX5 during the G1/S cell cycle phase, promoting DDX5 protein stability.

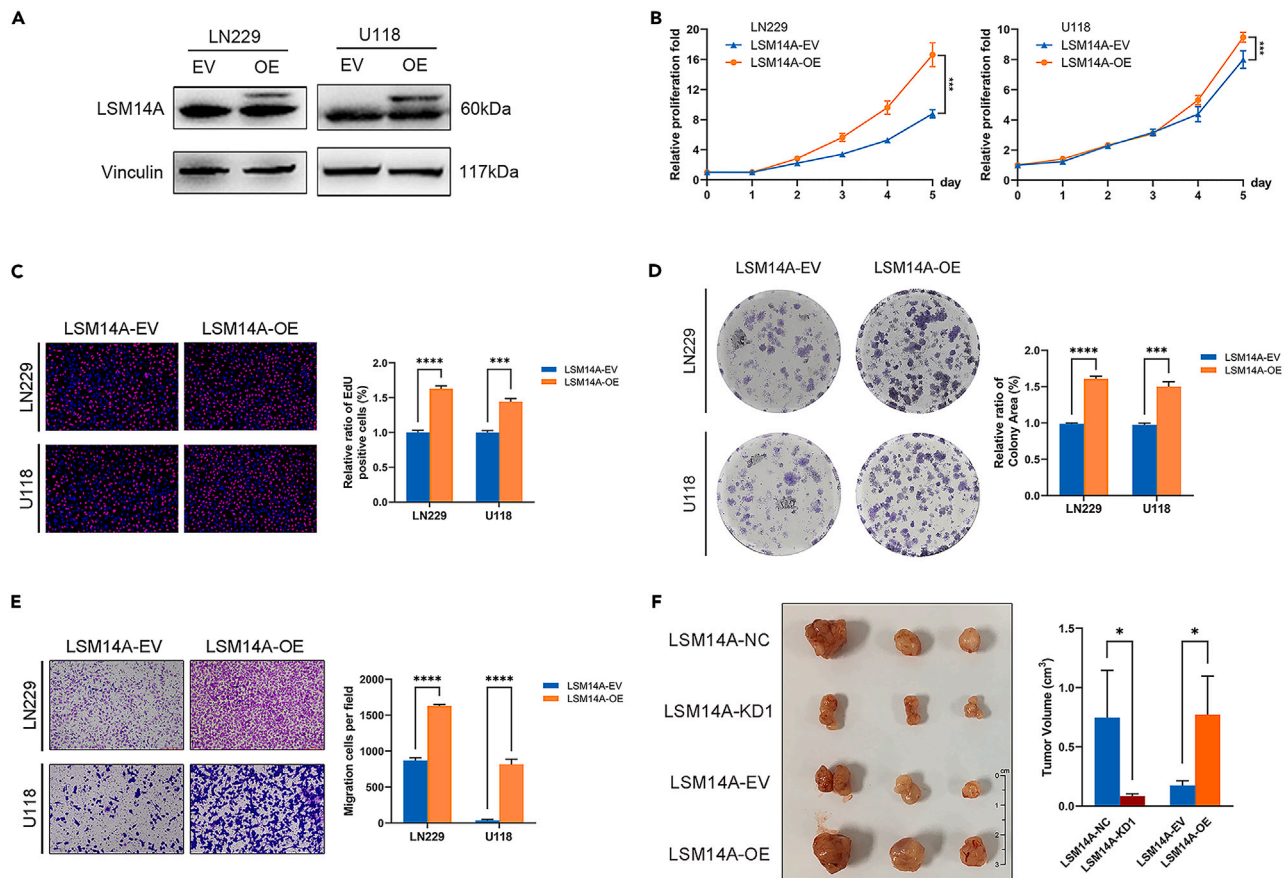


Figure 3. LSM14A overexpression augments GBM cell proliferation and migration

(A) Efficiency of LSM14A overexpression at the protein level in LN229 and U118 cells.

(B–D) Cell proliferation in LN229 and U118 cells overexpressing LSM14A was assessed via CCK-8 (B), EdU (C), and colony formation (D) assays. Differences between LSM14A-EV and LSM14A-OE were quantified.

(E) The migration capability of LN229 and U118 cells overexpressing LSM14A was evaluated using a Transwell assay.

(F) Left: Images showcase tumors from each mice group, right: statistical analysis of the tumor weights from each group revealed a significant difference. The data are represented as the mean \pm S.D. of three independent experiments. * $p < 0.05$, *** $p < 0.001$, **** $p < 0.0001$.

LSM14A-mediated phenotypic alterations in GBM cells involve DDX5

To elucidate the role of DDX5 in these phenotypes, we conducted experiments across various cellular contexts. As noted earlier, LSM14A knockdown notably influenced the proliferation and migration of U87 and U251 GBM cells. However, overexpressing DDX5 after LSM14A knockdown partially reversed these effects, as evidenced by CCK-8, EdU, and transwell assays (Figure 5A–5C). Western blot (WB) assays indicated that the expression levels of CDK4 and P21 were also partially restored, showing LSM14A regulation through DDX5 (Figure 5D). Concurrently, we assessed the expression levels of proteins involved in migration pathways within this experimental context. The findings indicated a partial recovery in the expression of migration-related proteins (Figure S2J). In LSM14A knockout U87 and U251 cells, cell proliferation and migration were substantially inhibited, but overexpressing DDX5 still led to partial phenotypic restoration (Figure 5E–5G). WB experiments reaffirmed the regulatory effect of LSM14A on CDK4 and P21 via DDX5 (Figure 5H). In LN229 and U118 cells, DDX5 knockdown also partially counteracted the effects of LSM14A overexpression on proliferation and migration (Figure 5I–5K). Additionally, immunoblot analysis further underscored the interplay between LSM14A, DDX5, and their downstream effectors CDK4 and P21 (Figure 5L). And migration pathway-associated proteins similarly obtained results opposite to the experimental design of knockdown LSM14A while overexpressing DDX5 (Figure S2K). The data indicate that DDX5 mediates LSM14A-induced GBM cell proliferation and migration and that LSM14A modulates CDK4 and P21 protein levels via DDX5.

METTL1 binds to LSM14A mRNA and modulates its expression

While exploring the oncogenic mechanism of METTL1, we drew insights from the sequencing of global RNA by Esteban et al., which emphasized m⁷G methylation within LSM14A mRNA.³⁸ Consequently, we aimed to further explore the relationship between METTL1

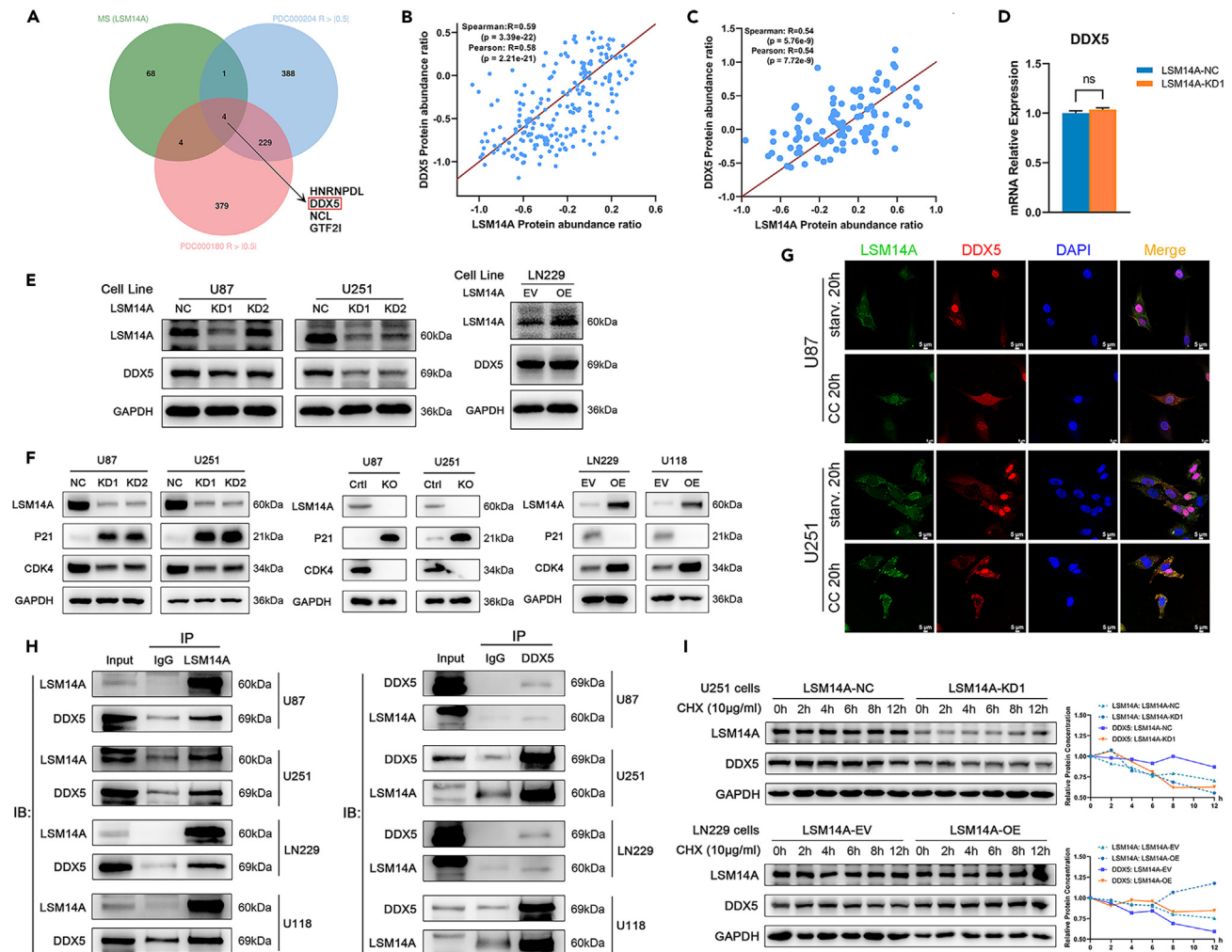


Figure 4. LSM14A and DDX5 interaction enhances DDX5 stability

(A) Venn diagram displaying LSM14A-interacting proteins identified through mass spectrometry and correlation analyses.

(B and C) Correlation analysis of LSM14A and DDX5 protein levels in the PDC000180 (B) and PDC000204 (C) datasets.

(D) RT-qPCR analysis of DDX5 mRNA levels in LSM14A-KD1 U87 cells.

(E) Immunoblotting analysis highlighting differences in DDX5 protein levels in U87 and U251 cells with LSM14A knockdown and LN229 cells with LSM14A overexpression compared to controls.

(F) Immunoblot assessment of LSM14A, P21, and CDK4 protein expression in LSM14A knockdown or knockout U87 and U251 cells and in LSM14A-overexpressing LN229 and U118 cells.

(G) Immunofluorescence images depicting LSM14A (green), DDX5 (red), and DAPI-stained nuclei (blue) in cells at different phases of the cell cycle after 20h of starvation (starv.) or regular (CC) culture conditions.

(H) CoIP assay to examine endogenous LSM14A and DDX5 interaction in U87, U251, LN229, and U118 cells. Left panel: LSM14A binding to DDX5 detected using an anti-LSM14A antibody; Right panel: DDX5 binding to LSM14A identified using an anti-DDX5 antibody.

(I) Immunoblotting analyses of DDX5 protein half-life in LSM14A knockdown U251 cells and LSM14A overexpressing LN229 cells, right: grayscale value statistics.

and LSM14A. Utilizing multiple databases, we validated our previous observations: overexpression of METTL1 in GBM is associated with unfavorable patient outcomes (Figures S3A and S3B). Using the PDC000204 dataset, we examined the association between METTL1 protein and LSM14A mRNA expression. The analysis identified a significant correlation in their expression (Figure S3C). Furthermore, cellular models indicated a potential regulatory role of METTL1 in LSM14A expression levels. Specifically, RT-qPCR demonstrated reduced LSM14A mRNA expression upon METTL1 knockdown (Figure 6A), while immunoblotting revealed LSM14A protein level changes based on METTL1 expression (Figure 6B). RIP experiments confirmed the binding of METTL1 protein to LSM14A mRNA (Figure S3D). Furthermore, MeRIP revealed m⁷G modification in LSM14A mRNA (Figure 6C). These findings suggest that METTL1 could modulate LSM14A expression via m⁷G modification.

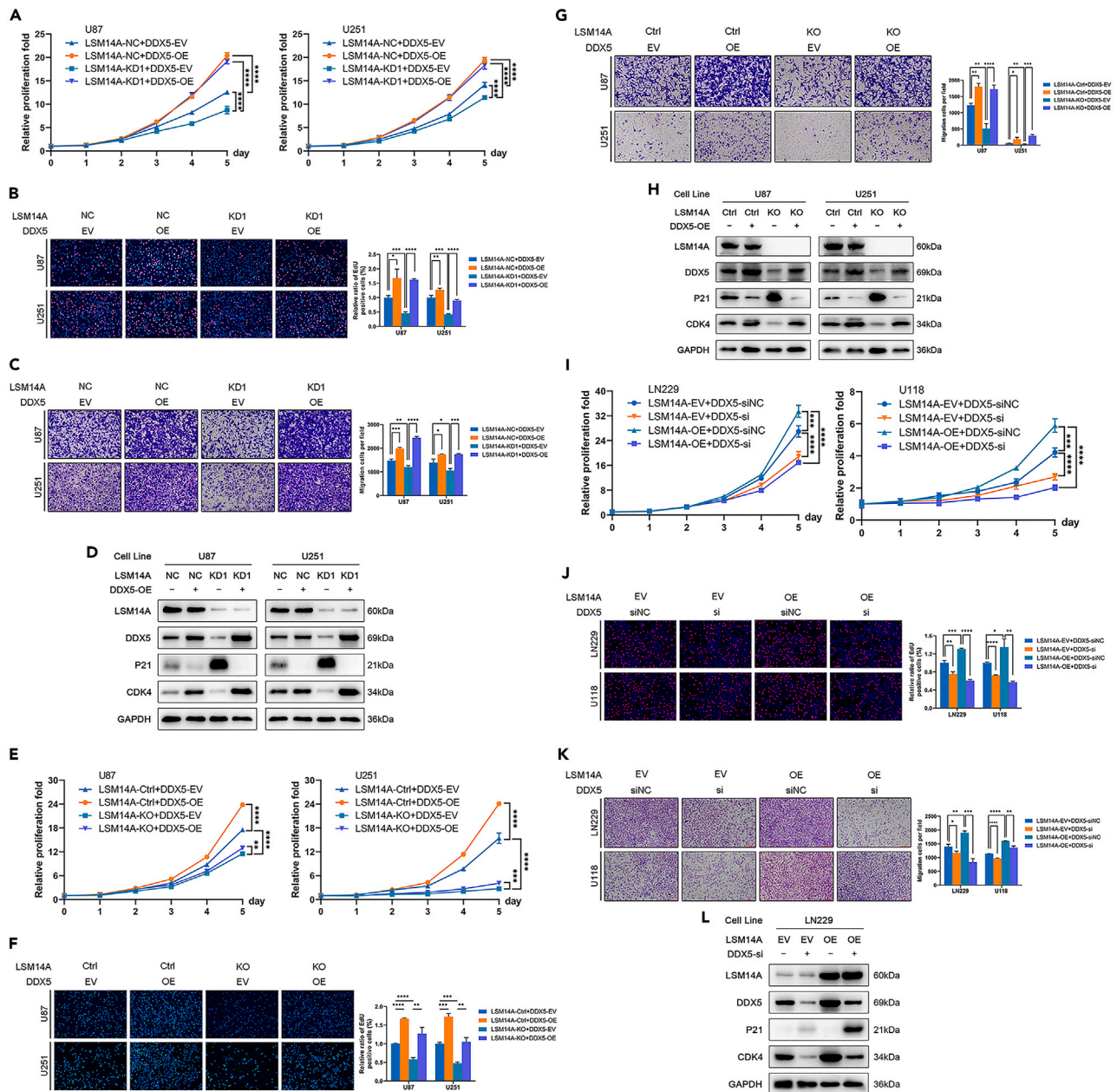


Figure 5. LSM14A-mediated proliferation and migration through DDX5

(A–C) Proliferation (A and B) and migration (C) in U87 and U251 cells overexpressing DDX5 with LSM14A knockdown. (D) Immunoblot analysis of CDK4 and P21 expression upon DDX5 overexpression following LSM14A knockdown. (E–G) Proliferation (E and F) and migration (G) in U87 and U251 cells overexpressing DDX5 after LSM14A knockdown and quantitatively analyzed. (H) Immunoblot analysis of CDK4 and P21 levels after DDX5 overexpression in LSM14A-knockdown cells. (I–K) Proliferation (I and J) and migration (K) in LN229 and U118 cells with DDX5 knockdown overexpressing LSM14A and quantitatively analyzed. (L) Immunoblot analysis of CDK4 and P21 levels in LN229 cells after DDX5 knockdown and LSM14A overexpression. The data are represented as the mean \pm S.D. of three independent experiments. * $p < 0.05$, ** $p < 0.01$, *** $p < 0.001$, **** $p < 0.0001$.

LSM14A mediates METTL1-Induced phenotypic changes in GBM cells

To investigate whether LSM14A mediates the METTL1-induced GBM cell phenotype, we adjusted LSM14A expression in cells with METTL1 knockdown or overexpression. In U87 and LN229 cell contexts, altering LSM14A expression modulated the effects of METTL1 on GBM cell proliferation (Figures 6D and 6E). We also discerned this reversal via the EdU staining assay (Figures 6F and 6G). Notably, LSM14A expression adjustments also impacted the influence of METTL1 on GBM cell migration (Figures 6H and 6I). Deepening our understanding, we found that

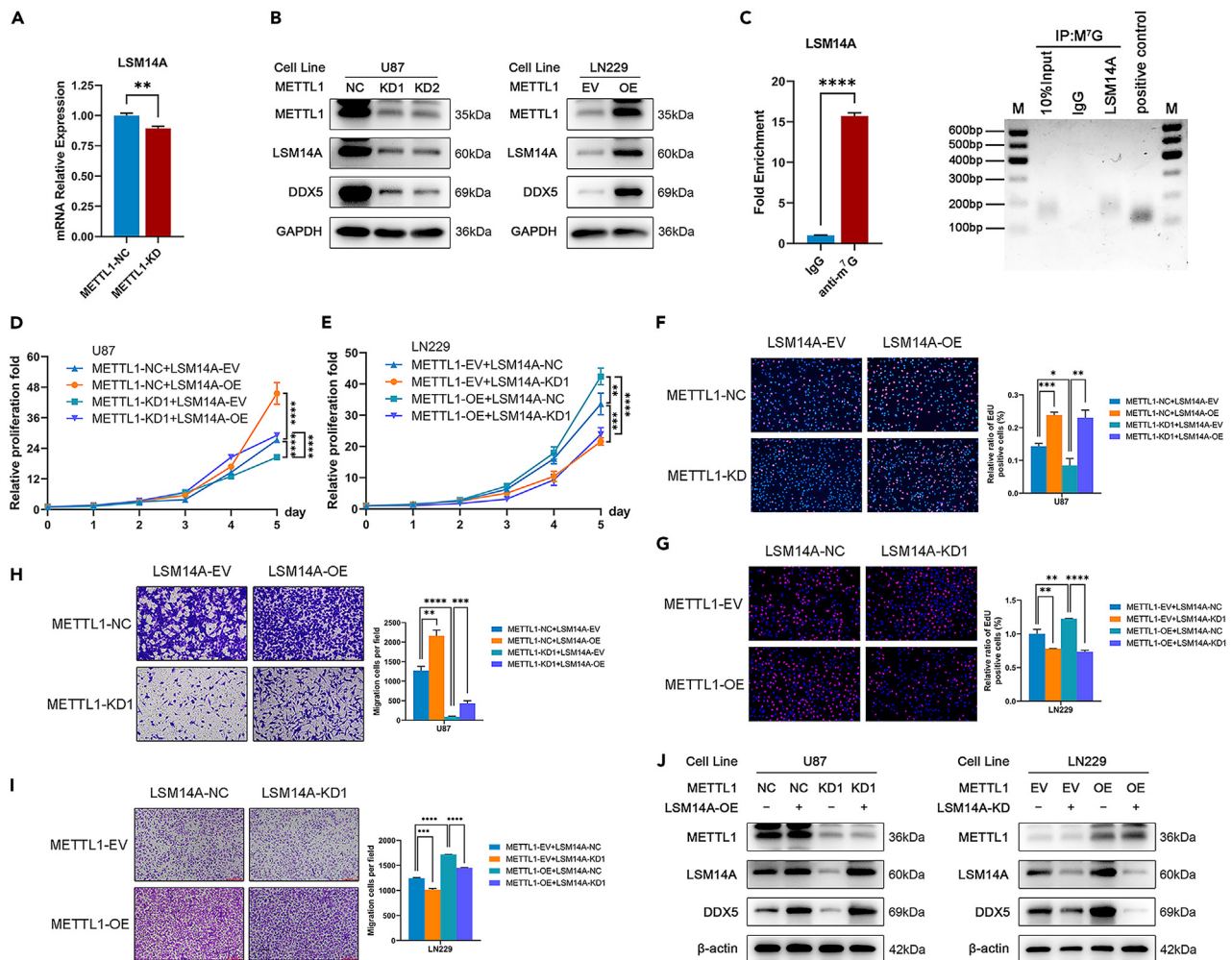


Figure 6. METTL1 regulates LSM14A-induced proliferation and migration, acting upstream of LSM14A

(A) RT-qPCR detected LSM14A mRNA levels in U87 cells with METTL1 knockdown. (B) Levels of LSM14A and DDX5 proteins in U87 cells with METTL1 knockdown (left panel) and LN229 cells overexpressing METTL1 were analyzed using immunoblotting. (C) The MeRIP assay detected m⁷G modifications in LSM14A mRNA. RT-qPCR was used to assess the enrichment efficiency of LSM14A mRNA (right panel: DNA gel electrophoresis results). (D–I) Effects of LSM14A expression regulation on cell proliferation (D–G) and migration (H and I) based on METTL1 modulation. (J) The effect of LSM14A expression regulation on DDX5 protein levels in U87 and LN229 cells with METTL1 modulation was determined by immunoblotting. The data are represented as the mean ± S.D. of three independent experiments. **p* < 0.05, ***p* < 0.01, ****p* < 0.001, *****p* < 0.0001.

LSM14A mediates the regulatory role of METTL1 on DDX5 (Figure 6J). Lastly, Western blot analyses of 15 clinical samples confirmed a consistent expression trend among METTL1, LSM14A, and DDX5 (Figure S3E). In conclusion, METTL1 modulates LSM14A expression, positioning LSM14A as a mediator in the METTL1-directed regulation of GBM cell proliferation and migration.

DISCUSSION

As illustrated in Figure 7, this study examines the critical role of the METTL1-LSM14A-DDX5 signaling pathway in cell proliferation and migration. The signaling process begins with METTL1 binding to LSM14A mRNA, subsequently elevating LSM14A expression levels. During the G1/S transition, DDX5 relocates from the nucleus to the cytoplasm to interact with LSM14A, which enhances DDX5 protein stability and promotes GBM cell proliferation and migration.

LSM14A is a vital component of P-bodies and SGs, facilitating various cellular processes. These processes include mRNA processing (such as degradation,³⁹ translocation,⁶ interference,^{40,41} and repression of translation activities),¹⁰ recognition of viral genetic materials,⁴² and facilitation of mitotic spindle assembly.¹² Previous research indicates a marked elevation in LSM14A expression in hepatocellular carcinoma, and

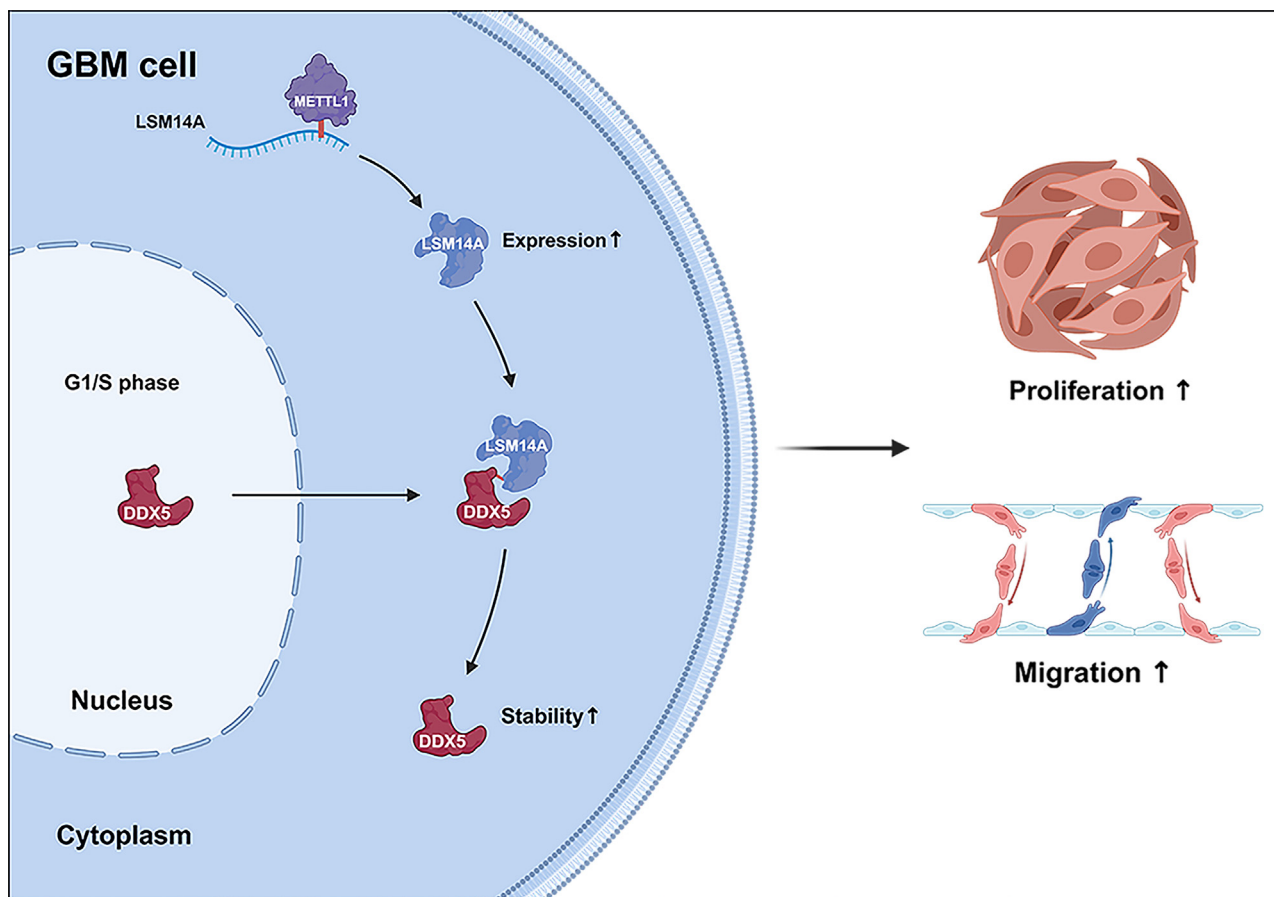


Figure 7. Schematic representation of the METTL1-LSM14A-DDX5 axis in mediating GBM cell proliferation and migration

the inhibition of LSM14A expression can curb the proliferation of these carcinoma cells.¹³ However, the precise mechanism by which LSM14A promotes tumor cell proliferation remains elusive. Notably, its functions and roles in brain tumors have yet to be explicitly reported. In this study, utilizing multiple published datasets and clinical samples, we illustrated that LSM14A acts as an oncogene in GBM and is significantly correlated with adverse patient prognosis. Alterations in LSM14A levels, including knockdown, knockout, or overexpression, markedly influence the proliferation and migration of GBM cells. Furthermore, pathway enrichment analysis revealed a significant correlation between LSM14A and the cell cycle, with LSM14A knockdown markedly increasing the proportion of GBM cells in the G1/S phase. These findings indicate a critical role of LSM14A in fostering the proliferation and migration of GBM cells.

Prior research indicates that the primary function of LSM14A in regulating mRNAs operates through protein-protein interactions.⁸ Through a thorough analysis involving mass spectrometry and database integration, we identified DDX5, a conserved member of the DEAD-box RNA helicase family, as a protein of interest. Notably, LSM14A has been known to interact with the RecA-like domain of DDX6,³⁵ suggesting a potential interaction with DDX5, given its conservation in the DDX family. DDX5 is implicated in a multitude of cellular activities, including RNA processing (splicing, translocation, and translation), DNA replication, viral infection, innate immunity, ribosome and miRNA biogenesis, and transcriptional regulation.^{15,22} It also plays a crucial role in tumorigenesis, particularly impacting the G1/S phase transition by modulating the cell cycle proteins P21 and CDK4.^{32–34} Our data indicate that LSM14A modulates the protein levels of DDX5 as well as its downstream molecules, CDK4 and P21. Before delving into the interaction between LSM14A and DDX5, we noted discrepancies in the subcellular localization of both proteins. LSM14A is predominantly localized in the cytoplasm.^{10,43} In contrast, DDX5 primarily localizes in the nucleus during the G0 phase and exhibits an increased presence in the cytoplasm during the G1/S phase. It aligns near condensed chromosomes in the M phase.⁴⁴ This led us to hypothesize that these proteins might interact mainly during the G1/S phase. Supporting this, our IF and colP experiments showed interactions in this phase. Notably, alterations in LSM14A expression did not impact DDX5 mRNA levels, suggesting that LSM14A potentially facilitates DDX5 expression through post-translational modifications. Existing studies suggest that LSM14A might stabilize interacting proteins within the cytoplasm.^{34–36} Our data reveal that LSM14A enhances DDX5 protein stability. A series of rescue experiments demonstrated the mediating role of DDX5 in LSM14A-induced proliferation, migration, and the regulation of CDK4 and P21 in GBM. Significantly, we found a negative correlation between DDX5 and the protein levels of P21, deviating from earlier research outcomes. Previous research has highlighted the role of DDX5 in enhancing P21 transcription.³¹ Interestingly, both LSM14A and DDX5 engage in mRNA processing activities (splicing,

transport, and translation), facilitated through mRNPs within the cytoplasm. LSM14A orchestrates mRNA degradation and translation by interfacing with pivotal proteins present in the mRNP granule P-body, including AGO2.³⁴ Conversely, during DDX5-facilitated nonsense-mediated mRNA decay (NMD), DDX5, and AGO2 colocalize within the P-body to govern mRNA degradation.⁴⁵ Consequently, we theorize that this potential interaction underlies the contrasting regulatory impacts of DDX5 on P21 observed at both the mRNA and protein levels, an aspect that warrants further experimental exploration.

METTL1 is a key RNA methyltransferase that, in conjunction with WDR4, forms the METTL1/WDR4 complex, modifying m⁷G in various RNAs, which in turn controls mRNA translation and cell cycle progression.⁴⁶ Our preceding research indicated that METTL1 serves as a significant oncogenic factor in GBM, stimulating GBM cell proliferation.³¹ Significantly, Esteban et al. uncovered a potential METTL1-mediated m⁷G methylation site within LSM14A mRNA.³⁸ A recent study indicated that METTL1 enhances the localization, stability, and translational repression of specific mRNAs in SGs of tumor cells via Quaking proteins (QKIs).³⁰ LSM14A is also a crucial component of SGs, similarly influencing mRNA localization.⁶ These findings prompted us to investigate the potential role of LSM14A in mediating the METTL1-induced GBM phenotype. We hypothesize that METTL1 modulates LSM14A mRNA levels via m⁷G methylation, thereby fostering GBM cell proliferation and migration. To substantiate this hypothesis, we initially reaffirmed the elevated expression of METTL1 in GBM by amalgamating sequencing results from various datasets; this trend strongly correlates with unfavorable patient prognosis. Experimental series confirmed the relationship between METTL1 and LSM14A, revealing a pronounced positive association between METTL1 protein and LSM14A mRNA. Further experiments validated the interaction between METTL1 protein and LSM14A mRNA, impacting both the mRNA and protein expression of LSM14A. Rescue experiments indicated that METTL1 promotes GBM cell proliferation and migration through LSM14A and adjusts downstream DDX5 protein levels.

In conclusion, our study demonstrates that LSM14A is an oncogene regulated by METTL1. During the G1/S phase, LSM14A interacts with nuclear translocated DDX5 in the cytoplasm, enhancing the protein stability of DDX5 and thereby promoting proliferation and migration in GBM. These initial findings establish a foundational platform for future detailed studies examining the roles of METTL1, LSM14A, and DDX5 in cell cycle progression, potentially deepening our understanding of GBM pathogenesis.

Limitations of the study

In this study, a detailed investigation is required to unravel the complex interaction between METTL1 and LSM14A mRNA, particularly the mechanisms governing specific mRNA m⁷G methylation regulation. Furthermore, to comprehensively elucidate the precise role of this mechanism in a physiological environment, a more extensive *in vivo* validation grounded in our *ex vivo* experiments is vital. Additionally, a deeper exploration of the post-translational modification mechanisms between LSM14A and DDX5, and their influence on overall cellular function warrants further investigation. Despite the study's limitations, our findings undeniably offer fresh insights into deciphering the molecular regulatory network involved in GBM.

STAR★METHODS

Detailed methods are provided in the online version of this paper and include the following:

- [KEY RESOURCES TABLE](#)
- [RESOURCE AVAILABILITY](#)
 - Lead contact
 - Materials availability
 - Data and code availability
- [EXPERIMENTAL MODEL AND STUDY PARTICIPANT DETAILS](#)
 - Clinical specimen and ethical statement
 - Cell lines and cell culture
 - Xenograft tumor assay
- [METHOD DETAILS](#)
 - Data source
 - Plasmids, shRNAs, and siRNAs
 - CRISPR-mediated LSM14A knockout
 - Western blot analysis (WB)
 - Cell proliferation detection
 - Flow cytometry for cell cycle analysis
 - Wound-healing and transwell assays
 - Immunofluorescence (IF)
 - Subcellular protein fractionation assay
 - Protein coimmunoprecipitation assay (Co-IP)
 - Protein half-life assay
 - RNA immunoprecipitation assay (RIP)
 - Methylated RNA immunoprecipitation assay (MeRIP)

- RT-qPCR analysis
- **QUANTIFICATION AND STATISTICAL ANALYSIS**
- Statistical analysis

SUPPLEMENTAL INFORMATION

Supplemental information can be found online at <https://doi.org/10.1016/j.isci.2024.110225>.

ACKNOWLEDGMENTS

We would like to thank other members of the Immunology Laboratory at China Medical University for their discussions and comments. This work was supported by the Science and Technology Foundation of Liaoning of China [grant numbers 2023JH2/101300045].

AUTHOR CONTRIBUTIONS

G.L. conceived and designed the study. C.W. and Y.H. performed the bioinformatics analysis and *in vitro* experiments and contributed equally to this work as co-first authors. X.F. and S.Z. were responsible for experimental animal grouping and *in vivo* experiments. J.H., L.L., and D.Z. analyzed and validated the data. G.L. drafted and wrote the manuscript.

DECLARATION OF INTERESTS

The authors declare no competing interests.

Received: October 30, 2023

Revised: February 6, 2024

Accepted: June 6, 2024

Published: June 8, 2024

REFERENCES

1. Ostrom, Q.T., Cioffi, G., Gittleman, H., Patil, N., Waite, K., Kruchko, C., and Barnholtz-Sloan, J.S. (2019). CBTRUS Statistical Report: Primary Brain and Other Central Nervous System Tumors Diagnosed in the United States in 2012-2016. *Neuro Oncol.* 21, v1–v100. <https://doi.org/10.1093/neuonc/noz150>.
2. Aldape, K., Brindle, K.M., Chesler, L., Chopra, R., Gajjar, A., Gilbert, M.R., Gottardo, N., Gutmann, D.H., Hargrave, D., Holland, E.C., et al. (2019). Challenges to curing primary brain tumors. *Nat. Rev. Clin. Oncol.* 16, 509–520. <https://doi.org/10.1038/s41571-019-0177-5>.
3. Molinaro, A.M., Taylor, J.W., Wiencke, J.K., and Wrensch, M.R. (2019). Genetic and molecular epidemiology of adult diffuse glioma. *Nat. Rev. Neurol.* 15, 405–417. <https://doi.org/10.1038/s41582-019-0220-2>.
4. Cloughesy, T.F., Cavenee, W.K., and Mischel, P.S. (2014). Glioblastoma: from molecular pathology to targeted treatment. *Annu. Rev. Pathol.* 9, 1–25. <https://doi.org/10.1146/annurev-pathol-011110-130324>.
5. Lim, M., Xia, Y., Bettegowda, C., and Weller, M. (2018). Current state of immunotherapy for glioblastoma. *Nat. Rev. Clin. Oncol.* 15, 422–442. <https://doi.org/10.1038/s41571-018-0003-5>.
6. Yang, W.H., Yu, J.H., Gulick, T., Bloch, K.D., and Bloch, D.B. (2006). RNA-associated protein 55 (RAP55) localizes to mRNA processing bodies and stress granules. *RNA* 12, 547–554. <https://doi.org/10.1261/rna.2302706>.
7. Song, D., Kuang, L., Yang, L., Wang, L., Li, H., Li, X., Zhu, Z., Shi, C., Zhu, H., and Gong, W. (2022). Yin and yang regulation of stress granules by Caprin-1. *USA* 119, e2207975119. <https://doi.org/10.1073/pnas.2207975119>.
8. Lieb, B., Carl, M., Hock, R., Gebauer, D., and Scheer, U. (1998). Identification of a novel mRNA-associated protein in oocytes of *Pleurodeles waltl* and *Xenopus laevis*. *Exp. Cell Res.* 245, 272–281. <https://doi.org/10.1006/excr.1998.4249>.
9. Minshall, N., Reiter, M.H., Weil, D., and Standart, N. (2007). CPEB interacts with an ovary-specific eIF4E and 4E-T in early *Xenopus* oocytes. *J. Biol. Chem.* 282, 37389–37401. <https://doi.org/10.1074/jbc.M704629200>.
10. Tanaka, K.J., Ogawa, K., Takagi, M., Imamoto, N., Matsumoto, K., and Tsujimoto, M. (2006). RAP55, a cytoplasmic mRNP component, represses translation in *Xenopus* oocytes. *J. Biol. Chem.* 281, 40096–40106. <https://doi.org/10.1074/jbc.M609059200>.
11. Li, Y., Chen, R., Zhou, Q., Xu, Z., Li, C., Wang, S., Mao, A., Zhang, X., He, W., and Shu, H.B. (2012). LSM14A is a processing body-associated sensor of viral nucleic acids that initiates cellular antiviral response in the early phase of viral infection. *Proc. Natl. Acad. Sci. USA* 109, 11770–11775.
12. Mili, D., Georgesse, D., and Kenani, A. (2015). Localization and role of RAP55/LSM14 in HeLa cells: a new finding on the mitotic spindle assembly. *Acta Biochim. Pol.* 62, 613–619. https://doi.org/10.18388/abp.2015_1107.
13. Zhuang, H., Chen, B., Tang, C., Chen, X., Tan, W., Yang, L., Xie, Z., Ma, X., Wang, Q., Zhang, C., et al. (2022). Identification of LSM Family Members as Novel Unfavorable Biomarkers in Hepatocellular Carcinoma. *Front. Oncol.* 12, 871771.
14. Zhang, L., and Li, X. (2021). DEAD-Box RNA Helicases in Cell Cycle Control and Clinical Therapy. *Cells* 10, 1540. <https://doi.org/10.3390/cells10061540>.
15. Nyamao, R.M., Wu, J., Yu, L., Xiao, X., and Zhang, F.M. (2019). Roles of DDX5 in the tumorigenesis, proliferation, differentiation, metastasis and pathway regulation of human malignancies. *Biochim. Biophys. Acta. Rev. Cancer* 1871, 85–98. <https://doi.org/10.1016/j.bbcan.2018.11.003>.
16. Wang, Z., Luo, Z., Zhou, L., Li, X., Jiang, T., and Fu, E. (2015). DDX5 promotes proliferation and tumorigenesis of non-small-cell lung cancer cells by activating beta-catenin signaling pathway. *Cancer Sci.* 106, 1303–1312. <https://doi.org/10.1111/cas.12755>.
17. Guturi, K.K.N., Sarkar, M., Bhowmik, A., Das, N., and Ghosh, M.K. (2014). DEAD-box protein p68 is regulated by β -catenin/transcription factor 4 to maintain a positive feedback loop in control of breast cancer progression. *Breast Cancer Res.* 16, 496.
18. Sha, M., Lin, M., Wang, J., Ye, J., Xu, J., Xu, N., and Huang, J. (2018). Long non-coding RNA MIAT promotes gastric cancer growth and metastasis through regulation of miR-141/DDX5 pathway. *J. Exp. Clin. Cancer Res.* 37, 58.
19. Wang, R., Jiao, Z., Li, R., Yue, H., and Chen, L. (2012). p68 RNA helicase promotes glioma cell proliferation *in vitro* and *in vivo* via direct regulation of NF- κ B transcription factor p50. *Neuro Oncol.* 14, 1116–1124. <https://doi.org/10.1093/neuonc/nos131>.
20. Zheng, Y., Lei, T., Jin, G., Guo, H., Zhang, N., Chai, J., Xie, M., Xu, Y., Wang, T., Liu, J., et al. (2021). LncPSCA in the 8q24.3 risk locus drives gastric cancer through destabilizing DDX5. *EMBO Rep.* 22, e52707.
21. Mooney, S.M., Grande, J.P., Salisbury, J.L., and Janknecht, R. (2010). Sumoylation of p68 and p72 RNA helicases affects protein stability and transactivation potential.

- Biochemistry 49, 1–10. <https://doi.org/10.1021/bi901263m>.
22. Li, F., Ling, X., Chakraborty, S., Fountzilias, C., Wang, J., Jamroze, A., Liu, X., Kalinski, P., and Tang, D.G. (2023). Role of the DEAD-box RNA helicase DDX5 (p68) in cancer DNA repair, immune suppression, cancer metabolic control, virus infection promotion, and human microbiome (microbiota) negative influence. *J. Exp. Clin. Cancer Res.* 42, 213. <https://doi.org/10.1186/s13046-023-02787-x>.
 23. Mazurek, A., Luo, W., Krasnitz, A., Hicks, J., Powers, R.S., and Stillman, B. (2012). DDX5 regulates DNA replication and is required for cell proliferation in a subset of breast cancer cells. *Cancer Discov.* 2, 812–825.
 24. Li, Y., Liu, X., Cui, X., Tan, Y., Wang, Q., Wang, Y., Xu, C., Fang, C., and Kang, C. (2021). LncRNA PRADX-mediated recruitment of PRC2/DDX5 complex suppresses UBXN1 expression and activates NF- κ B activity, promoting tumorigenesis. *Theranostics* 11, 4516–4530.
 25. Wang, T., Cao, L., Dong, X., Wu, F., De, W., Huang, L., and Wan, Q. (2020). LINC01116 promotes tumor proliferation and neutrophil recruitment via DDX5-mediated regulation of IL-1 β in glioma cell. *Cell Death Dis.* 11, 302. <https://doi.org/10.1038/s41419-020-2506-0>.
 26. Wang, R., Bao, H.B., Du, W.Z., Chen, X.F., Liu, H.L., Han, D.Y., Wang, L.G., Wu, J.N., Wang, C.L., Yang, M.C., et al. (2019). P68 RNA helicase promotes invasion of glioma cells through negatively regulating DUSP5. *Cancer Sci.* 110, 107–117.
 27. Lin, S., Liu, Q., Lelyveld, V.S., Choe, J., Szostak, J.W., and Gregory, R.I. (2018). Mettl1/Wdr4-Mediated m(7)G tRNA Methylome Is Required for Normal mRNA Translation and Embryonic Stem Cell Self-Renewal and Differentiation. *Mol. Cell* 71, 244–255.e5.
 28. Pandolfini, L., Barbieri, I., Bannister, A.J., Hendrick, A., Andrews, B., Webster, N., Murat, P., Mach, P., Brandi, R., Robson, S.C., et al. (2019). METTL1 Promotes let-7 MicroRNA Processing via m7G Methylation. *Mol. Cell* 74, 1278–1290.e9. <https://doi.org/10.1016/j.molcel.2019.03.040>.
 29. Huang, Y., Ma, J., Yang, C., Wei, P., Yang, M., Han, H., Chen, H.D., Yue, T., Xiao, S., Chen, X., et al. (2022). METTL1 promotes neuroblastoma development through m(7)G tRNA modification and selective oncogenic gene translation. *Biomark. Res.* 10, 68.
 30. Zhao, Z., Qing, Y., Dong, L., Han, L., Wu, D., Li, Y., Li, W., Xue, J., Zhou, K., Sun, M., et al. (2023). QKI shuttles internal m(7)G-modified transcripts into stress granules and modulates mRNA metabolism. *Cell* 186, 3208–3226.e27.
 31. Li, L., Yang, Y., Wang, Z., Xu, C., Huang, J., and Li, G. (2021). Prognostic role of METTL1 in glioma. *Cancer Cell Int.* 21, 633. <https://doi.org/10.1186/s12935-021-02346-4>.
 32. Bates, G.J., Nicol, S.M., Wilson, B.J., Jacobs, A.M.F., Bourdon, J.C., Wardrop, J., Gregory, D.J., Lane, D.P., Perkins, N.D., and Fuller-Pace, F.V. (2005). The DEAD box protein p68: a novel transcriptional coactivator of the p53 tumour suppressor. *EMBO J.* 24, 543–553. <https://doi.org/10.1038/sj.emboj.7600550>.
 33. Nicol, S.M., Bray, S.E., Black, H.D., Lorimore, S.A., Wright, E.G., Lane, D.P., Meek, D.W., Coates, P.J., and Fuller-Pace, F.V. (2013). The RNA helicase p68 (DDX5) is selectively required for the induction of p53-dependent p21 expression and cell-cycle arrest after DNA damage. *Oncogene* 32, 3461–3469.
 34. Fu, Q., Song, X., Liu, Z., Deng, X., Luo, R., Ge, C., Li, R., Li, Z., Zhao, M., Chen, Y., et al. (2017). miRomics and Proteomics Reveal a miR-296-3p/PRKCA/FAK/Ras/c-Myc Feedback Loop Modulated by HDGF/DDX5/ β -catenin Complex in Lung Adenocarcinoma. *Clin. Cancer Res.* 23, 6336–6350. <https://doi.org/10.1158/1078-0432.CCR-16-2813>.
 35. Kakumani, P.K., Harvey, L.M., Houle, F., Guitart, T., Gebauer, F., and Simard, M.J. (2020). CSDE1 controls gene expression through the miRNA-mediated decay machinery. *Life Sci. Alliance* 3, e201900632.
 36. Brandmann, T., Fakim, H., Padamsi, Z., Youn, J.Y., Gingras, A.C., Fabian, M.R., and Jinek, M. (2018). Molecular architecture of LSM14 interactions involved in the assembly of mRNA silencing complexes. *EMBO J.* 37, e97869. <https://doi.org/10.15252/embj.201797869>.
 37. Kruger, T., Hofweber, M., and Kramer, S. (2013). SCD6 induces ribonucleoprotein granule formation in trypanosomes in a translation-independent manner, regulated by its Lsm and RGG domains. *Mol. Biol. Cell* 24, 2098–2111. <https://doi.org/10.1091/mbc.E13-01-0068>.
 38. Orellana, E.A., Liu, Q., Yankova, E., Pirouz, M., De Braekeleer, E., Zhang, W., Lim, J., Aspris, D., Sendinc, E., Garyfallos, D.A., et al. (2021). METTL1-mediated m(7)G modification of Arg-TCT tRNA drives oncogenic transformation. *Mol. Cell* 81, 3323–3338.e14. <https://doi.org/10.1016/j.molcel.2021.06.031>.
 39. Bloch, D.B., Nobre, R.A., Bernstein, G.A., and Yang, W.H. (2011). Identification and characterization of protein interactions in the mammalian mRNA processing body using a novel two-hybrid assay. *Exp. Cell Res.* 317, 2183–2199. <https://doi.org/10.1016/j.yexcr.2011.05.027>.
 40. Kamenska, A., Simpson, C., Vindry, C., Broomhead, H., Bénard, M., Ernoult-Lange, M., Lee, B.P., Harries, L.W., Weil, D., and Standart, N. (2016). The DDX6-4E-T interaction mediates translational repression and P-body assembly. *Nucleic Acids Res.* 44, 6318–6334. <https://doi.org/10.1093/nar/gkw565>.
 41. Marnef, A., Sommerville, J., and Ladomery, M.R. (2009). RAP55: insights into an evolutionarily conserved protein family. *Int. J. Biochem. Cell Biol.* 41, 977–981.
 42. Li, Z., Chen, R., Zhao, J., Qi, Z., Ji, L., Zhen, Y., and Liu, B. (2015). LSM14A inhibits porcine reproductive and respiratory syndrome virus (PRRSV) replication by activating IFN- β signaling pathway in Marc-145. *Mol. Cell. Biochem.* 399, 247–256. <https://doi.org/10.1007/s11010-014-2251-8>.
 43. Rasch, F., Weber, R., Izaurralde, E., and Igrreja, C. (2020). 4E-T-bound mRNAs are stored in a silenced and deadenylated form. *Genes Dev.* 34, 847–860. <https://doi.org/10.1101/gad.336073.119>.
 44. Choi, Y.J., and Lee, S.G. (2012). The DEAD-box RNA helicase DDX3 interacts with DDX5, co-localizes with it in the cytoplasm during the G2/M phase of the cycle, and affects its shuttling during mRNP export. *J. Cell. Biochem.* 113, 985–996. <https://doi.org/10.1002/jcb.23428>.
 45. Geißler, V., Altmeyer, S., Stein, B., Uhlmann-Schiffler, H., and Stahl, H. (2013). The RNA helicase Ddx5/p68 binds to hUpf3 and enhances NMD of Ddx17/p72 and Smg5 mRNA. *Nucleic Acids Res.* 41, 7875–7888. <https://doi.org/10.1093/nar/gkt538>.
 46. Cheng, W., Gao, A., Lin, H., and Zhang, W. (2022). Novel roles of METTL1/WDR4 in tumor via m(7)G methylation. *Mol. Ther. Oncolytics* 26, 27–34. <https://doi.org/10.1016/j.omto.2022.05.009>.

STAR★METHODS

KEY RESOURCES TABLE

REAGENT or RESOURCE	SOURCE	IDENTIFIER
Antibodies		
anti-RAP55/LSM14A	Santa cruz	Cat# sc-398552; RRID: AB_3099527
anti-DDX5	Abcam	Cat# ab126730; RRID: AB_11130291
anti-METTL1	Thermo Fisher Scientific	Cat# PA5-80810; RRID: AB_2788084
anti-GAPDH	Bioss	Cat# bs-2188R; RRID: AB_10856675
anti-LSM14A	Proteintech	Cat# 18336-1-AP; RRID: AB_10644339
anti-CDK4	Proteintech	Cat# 11026-1-AP; RRID: AB_2078702
anti-P21	Proteintech	Cat# 10355-1-AP; RRID: AB_2077682
anti-snail	Proteintech	Cat# 13099-1-AP; RRID: AB_2191756
anti-IgG	Proteintech	Cat# B900620; RRID: AB_2883054
anti-vinculin	Proteintech	Cat# 66305-1-Ig; RRID: AB_2810300
anti-H3	Proteintech	Cat# 17168-1-AP; RRID: AB_2716755
anti- E-Cadherin	Abmart	Cat# TA0131; RRID: AB_2936787
anti- N-Cadherin	Abmart	Cat# T55015; RRID: AB_2937047
anti- ZO-1	Abmart	Cat# TA5145; RRID: AB_2936803
anti- Vimentin	Abmart	Cat# T55134; RRID: AB_2938551
Biological samples		
human glioma sample	Department of Neurosurgery, First Affiliated Hospital of China Medical University, Shenyang, Liaoning Province, China	N/A
Chemicals, peptides, and recombinant proteins		
cycloheximide	Selleck	N/A
RNAiso Plus	Takara	Cat# 9108/9109
crystal violet	Biosharp	Cat# 21155722
RIPA buffer	Beyotime	Cat# P0013B
PMSF	Beyotime	Cat# ST505
phosphatase inhibitor	Beyotime	Cat# P1082
Critical commercial assays		
BeyoClick™ EdU-488	Beyotime	Cat# C0071S
BeyoClick™ EdU-594	Beyotime	Cat# C0078S
Nuclear and Cytoplasmic Extraction Reagents	Thermo Scientific	Cat# 78833
Magna RIP Kit	Merck Millipore	Cat# 17-700
Reverse transcription and RT-qPCR kits	ABM	Cat# G592, G891, G892
m7G RNA Methylation Kit	GenSeq	Cat# GS-ET-004
Deposited data		
Genomic and clinical data from The Cancer Genome Atlas	UCSC Xena database	http://xena.ucsc.edu/
A cohort of 325 cases	Chinese Glioma Genome Atlas	http://www.cgga.org.cn
GBM proteomics datasets PDC000204	CPTAC	https://cptac-data-portal.georgetown.edu/cptac/s/S048 PDC000204

(Continued on next page)

Continued

REAGENT or RESOURCE	SOURCE	IDENTIFIER
GBM proteomics datasets PDC000180	CPTAC	https://cptac-data-portal.georgetown.edu/cptac/s/S048 PDC000180
Experimental models: Cell lines		
Human: U87 MG cells	National Collection of Authenticated Cell Cultures	N/A
Human: U251 cells	National Collection of Authenticated Cell Cultures	N/A
Human: LN229 cells	National Collection of Authenticated Cell Cultures	N/A
Human: U118 cells	National Collection of Authenticated Cell Cultures	N/A
Experimental models: Organisms/strains		
Mouse: BALB/c-nu	SiPeiFu	Cat# C201
Oligonucleotides		
shRNAs and gRNAs for LSM14A, see Table S1	This paper	N/A
siRNA for DDX5, see Table S1	This paper	N/A
shRNA for METTL1, see Table S1	This paper	N/A
Primers for LSM14A, see Table S2	This paper	N/A
Primers for DDX5, see Table S2	This paper	N/A
Primers for ACTB, see Table S2	This paper	N/A

RESOURCE AVAILABILITY

Lead contact

Further information and requests for resources and reagents should be directed to and will be fulfilled by the [lead contact](#), Guangyu Li (liguangyu1972@sina.com).

Materials availability

This study did not generate new unique reagents.

Data and code availability

- This paper analyzes existing, publicly available data. These accession numbers for the datasets are listed in the [key resources table](#). All data reported in this paper will be shared by the [lead contact](#) upon request.
- This paper does not report original code.
- Any additional information required to reanalyze the data reported in this paper is available from the [lead contact](#) upon request.

EXPERIMENTAL MODEL AND STUDY PARTICIPANT DETAILS

Clinical specimen and ethical statement

Fifteen human glioma samples, categorized as WHO grade I-III (9 samples) and WHO grade IV (6 samples), were procured from patients initially diagnosed with malignant gliomas at the Department of Neurosurgery, First Affiliated Hospital of China Medical University, Shenyang, Liaoning Province, China. The control group comprised paracancerous tissues sourced from 5 glioma patients. Detailed patient information from clinical sample sources is provided in [Table S4](#). The Ethics Committee of the First Affiliated Hospital of China Medical University granted approval for all clinical specimen collections (Ethical approval number for human participants: AF-SP-07-1.1-01). Written informed consent was obtained from each patient or their legal guardian.

Cell lines and cell culture

The human glioblastoma cell lines U87, U251, LN229, and U118 were obtained from the Chinese Academy of Sciences. All cell lines were accurately identified using STR analysis. Cells were cultured in high glucose Dulbecco's modified Eagle's medium (DMEM) (Gibco, No. C11995500bt) with 10% fetal bovine serum (Bioind, No. 04-001-1A) and a 1% antibiotic mixture (HyClone, No. SV30010) and maintained at 37°C and 5% CO₂ in a humidified incubator. Cells in the exponential growth phase were utilized for the experiments.

Xenograft tumor assay

All animal experiments followed the guidelines of the Animal Ethics Committee of China Medical University (Ethical approval number for animal participants: KT2022301). Six-week-old male BALB/c nude mice from the Department of Laboratory Animal Science of China Medical University (Shenyang, China) were subcutaneously injected with U87 and LN229 cells (5×10^5 in 10 μ L PBS) in quintets. Daily monitoring detected distress or neurological symptoms, leading to humane euthanasia when needed. Tumor tissues were measured at their largest cross-section. Volume was gauged as $V = (a \times b^2)/2$ ('a' and 'b' being the longest and shortest diameters, respectively). Mice near the end of life were euthanized using deep anesthesia. Others were humanely euthanized when their tumors reached a size considered ethically acceptable following injection.

METHOD DETAILS

Data source

Genomic and clinical data from The Cancer Genome Atlas (TCGA) were obtained from the UCSC Xena database (<http://xena.ucsc.edu/>). Duplicate samples from the same patient were excluded. A cohort of 325 cases, complete with clinical and molecular details, was obtained from the Chinese Glioma Genome Atlas (CGGA) database (<http://www.cgga.org.cn>). The GBM proteomics datasets PDC000204 and PDC000180 were sourced from the CPTAC database (<https://cptac-data-portal.georgetown.edu/cptac/s/S048>). RNA expression data for 276 glioma and 8 control samples were sourced from the GSE16011 dataset in the GEO database (<https://www.ncbi.nlm.nih.gov/geo/query/acc.cgi?acc=GSE16011>). Data were analyzed using R (version 4.1.0). The tidy, dplyr, and rtracklayer packages facilitated data cleaning and ID conversion.

Plasmids, shRNAs, and siRNAs

DDX5 or METTL1 was modulated in GBM cells through transfection using either plasmid (Genechem, Shanghai, China) or siRNA (Ribobio, No. R10043.8), employing Polyplus Invivo-jetPEI (Polyplus, France) as directed. To construct stable LSM14A-modulated cell lines, U87, U251, LN229, and U118 cells in logarithmic growth phase were transfected with lentivirus. Upon reaching 90% cell density, puromycin (2 μ g/ μ L) was added for selection. Stable colonies were propagated after 10–14 days. The efficacy of LSM14A modulation was evaluated by western blot analysis. The target sequences are listed in [Table S1](#).

CRISPR-mediated LSM14A knockout

The design of gRNA and the construction of the lentivirus for LSM14A knockout were conducted by Cyagen Biosciences. Four to five days after lentiviral infection, GBM cells were collected, and monoclonal cells were cultivated in 96-well plates by the limiting dilution method. Specific primers were tailored for the target exon region of the gRNA. Subsequently, monoclonal cells underwent screening for successful target exon knockout using RT-qPCR, with protein levels confirmed via Western blot (WB). The target sequences are listed in [Table S1](#).

Western blot analysis (WB)

Proteins were isolated using ice-cold RIPA buffer (Beyotime, P0013B), PMSF (Beyotime, Cat# ST505), and phosphatase inhibitor (Beyotime, Cat# P1082). Concentrations were determined with the BCA method. 50 μ g protein underwent 10% SDS-PAGE electrophoresis. After transfer to PVDF membranes (Millipore), membranes were blocked in nonfat milk (BD Pharmingen) and incubated with primary antibodies, followed by secondary antibody and visualization with chemiluminescence reagent (Beyotime, Cat# P0018AS). In the experiments conducted, antibodies were utilized as follows: anti-LSM14A/RAP55 (Santa Cruz, Cat# sc-398552), anti-DDX5 (Abcam, Cat# ab126730), anti-METTL1 (Thermo Fisher Scientific, Cat# PA5-80810), and anti-GAPDH (Bioss, Cat# bs-2188R). From Proteintech, China, we sourced anti-LSM14A (Cat# 18336-1-AP), anti-CDK4 (Cat# 11026-1-AP), anti-P21 (Cat# 10355-1-AP), anti-snail (Cat# 13099-1-AP), anti-IgG (Cat# B900620), anti-vinculin (Cat# 66305-1-Ig) and anti-Histone-H3 (Cat# 17168-1-AP). From abmart, China, we sourced anti-E-Cadherin (Cat# TA0131), anti-N-Cadherin (Cat# T55015), anti-ZO-1 (Cat# TA5145), anti-Vimentin (Cat# T55134).

Cell proliferation detection

For the CCK8 assay, cells (1,000/well) were incubated in 96-well plates at 37°C and 5% CO₂. Post-incubation, 10 μ L CCK8 was added and absorbance measured at 450 nm after 2 h. In the colony assay, 100 transfected cells were cultured in 12-well plates with 10% FBS for 2 weeks. Colonies were fixed, stained with 0.1% crystal violet (Biosharp, Cat# 21155722), and analyzed via ImageJ. EdU staining employed BeyoClick™ EdU-488 (Beyotime, Cat# C0071S) or EdU-594 (Beyotime, Cat# C0078S) kits, as per the kit's instructions. Fluorescence microscopy and ImageJ was used to determine EdU-positive cell percentages.

Flow cytometry for cell cycle analysis

Cells were cultured in 100 mm dishes (1×10^6 cells/dish) for 20 h, trypsinized, harvested, and washed with PBS. After centrifugation, the cells were resuspended in PBS + 5% BSA (Sigma, Cat# ST023), fixed in ethanol (4°C, 24 h), and resuspended in ribonuclease A (10 mg/ μ L). After staining with propidium iodide (37°C, 30 min), the cell cycle was analyzed with BD Biosciences FACSCalibur and FlowJo software (BD Biosciences, USA).

Wound-healing and transwell assays

Wound-healing assays were conducted using 12-well cell culture plates (Corning, USA). Scratches were made vertically at the center of each well with 10 μ L pipettes. The cells were then incubated for 0 h and 8 h in high-glucose DMEM without fetal bovine serum (FBS). Microscopic images were captured at 40 \times or 100 \times magnification, and gap area were measured using the software's plotting scale. The wound healing percentage was calculated for statistical analysis. For assessing invasion and migration, Transwell assays were utilized with cells placed in Transwell chambers (24-well format; Corning, USA). Invasion assays involved Matrigel-coated chambers (BD Biosciences, USA). Approximately $2-4 \times 10^4$ cells in 200 μ L of 2% FBS were added to the upper chamber, while the lower chamber had 600 μ L of 10% FBS medium. Following a 12-, 14-, or 18-h incubation at 37°C, the chambers were cleaned with PBS and fixed with 4% paraformaldehyde for 30 min. Cells on the membrane's top were removed, stained with crystal violet (room temperature, 30 min), rinsed with PBS, air-dried, and photographed.

Immunofluorescence (IF)

GBM cells (1×10^4 /well) were seeded in 24-well plates and incubated for 20 h. Cells were fixed with 4% paraformaldehyde, permeabilized using 0.1% Triton X-100, blocked with 3% BSA, and then incubated overnight at 4°C with primary antibodies (anti-LSM14A or anti-DDX5). This was followed by Alexa Fluor-conjugated secondary antibody exposure and DAPI staining (Sigma, Cat# D9542). Confocal microscopy images were analyzed with ImageJ.

Subcellular protein fractionation assay

The subcellular protein fractionation assay was performed using the Nuclear and Cytoplasmic Extraction Reagents (Thermo Scientific, Cat# 78833) according to the manufacturer's instructions. Collect 5×10^6 cells, add CER I, vortex 15s, incubate on ice 10 min. Add CER II, vortex 5s, ice incubate 1 min. Vortex 5s, centrifuge max speed 5 min. Transfer supernatant (cytoplasmic extract) to pre-cooled tube. Resuspend residual fraction in NER, vortex 15s, repeat every 10 min for 40 min. Centrifuge 10 min, transfer supernatant (nuclear extract) to new pre-cooled tube. Subject the extracts to Western blot analysis.

Protein coimmunoprecipitation assay (Co-IP)

For the endogenous Co-IP assay, cell lysates were prepared from U87, U251, LN229, or U118 cells. Coimmunoprecipitation was carried out using anti-LSM14A/RAP55 antibody, anti-DDX5 antibody, or control IgG as a negative control. This was followed by immunoblotting analysis using anti-LSM14A, anti-DDX5, and anti-CDK4 antibodies.

Protein half-life assay

U87, U251, and LN229 cells were treated under the indicated conditions, followed by the administration of 10 μ g/mL cycloheximide (CHX, Selleck, USA). Cell lysates were collected at defined time intervals (0, 2, 4, 6, 8, and 12 h) postexposure for analysis through Western blotting.

RNA immunoprecipitation assay (RIP)

The RNA immunoprecipitation assay was performed using the Magna RIP Kit (Merck Millipore, Cat# 17-700) according to the manufacturer's instructions. Approximately 2×10^7 cells underwent lysis, followed by RNA enrichment using 10 μ g of anti-METTTL1 antibody or IgG-loaded beads. The isolated RNA was subsequently purified and analyzed using RT-qPCR.

Methylated RNA immunoprecipitation assay (MeRIP)

The methylated RNA immunoprecipitation assay was performed using the m⁷G RNA Methylation Kit (GenSeq, Cat# GS-ET-004) according to the manufacturer's instructions. Adjust RNA concentration to 1 μ g/ μ L and dispense into PCR tubes. Fragment RNA with Fragmentation Buffer at 70°C for 6 min, then add Stop Buffer and cool. Combine samples, adjust volume, and add Buffer with ethanol for overnight precipitation. Next day, centrifuge to remove supernatant, then with 75% ethanol, and air-dry RNA. After solubilization, measure RNA size and concentration with Bioanalyzer. Separate RNA portion for input and remainder for immunoprecipitation. For immunoprecipitation, prepare magnetic beads, wash in IP buffer, and incubate with antibodies. Wash, then add MeRIP solution to beads and incubate at 4°C. Wash beads and incubate with RNA. After washing, resuspend in Buffer and transfer. Wash beads, add Buffer and ethanol, final wash, then collect RNA for MeRIP-qPCR.

RT-qPCR analysis

Total RNA was extracted with RNAiso Plus reagent (Takara, Cat# 9108/9109). Reverse transcription and RT-qPCR kits from ABM (Cat# G592, G891, G892) were used per manufacturer's guidelines. RT-qPCR cycling included 95°C (3 min), 95°C (15 s), and 60°C (1 min) for 40 cycles. Expression was determined using the $2^{-\Delta\Delta C_t}$ method. Primers, listed in [Table S2](#), were from Sangon Bio Inc., China.

QUANTIFICATION AND STATISTICAL ANALYSIS

Statistical analysis

To compare two conditions, a Student's t test was utilized. For analyses involving multiple comparisons, analysis of variance (ANOVA) accompanied by Bonferroni or Newman-Keuls correction was conducted. Values presenting a p value <0.05 were considered significant. Data were analyzed using GraphPad Prism version 9, with results presented as the mean \pm standard deviation (SD). The significance levels were marked as follows: * $p < 0.05$; ** $p < 0.01$; *** $p < 0.001$; **** $p < 0.0001$.